学位論文

「Hypoxia-mediated cancer stem cells in pseudopalisades with activation of hypoxia-inducible factor-1α/Akt axis in glioblastoma」

(膠芽腫の低酸素環境における HIF-1α/Akt 系依存性がん幹細胞化機構の証明)

ＤＭ１２００７　　犬飼　円

北里大学大学院医療系研究科医学専攻博士課程
臨床医科学群　脳神経外科学
指導教授　隈部　俊宏

著者の宣言

本学位論文は、著者の責任において実験を遂行し、得られた真実の結果に基づいて正確に作成したものに相違ないことをここに宣言する。

Abstract

Pseudopalisades (Ps) around necrotic foci are severely hypoxic and overexpress hypoxia-inducible factor (HIF) in glioblastoma (GBM). Hypoxic regions have been proposed as one of several distinct niches for cancer stem cells (CSCs) in GBM, but little is known about the association between Ps features and CSC properties. Herein, we focused on the biological role of Ps lesions. In clinical cases of GBM, expression of hypoxia-related molecules including HIF-1 α, Glut-1, $p27^{Kip1}$ as well as pAkt, was significantly increased in perinecrotic Ps lesions compared with non-necrotic areas and perinecrotic lesions lacking Ps features. Significantly higher expression levels of several CSC-related markers, including CD133, Sox2, CD44s, and aldehyde dehydrogenase (ALDH) 1, were also observed in Ps lesions, which were positively correlated with expression of hypoxia-related molecules and pAkt. Ps lesions also showed increased number of apoptotic cells and decreased bcl-2 and survivin expression compared with the surrounding tissue. Short-term exposure of astrocytoma cell lines to cobalt chloride ($CoCl_2$), which is known to mimic the effect of hypoxia, caused an increase in expression of both hypoxia- and CSC-related markers, in line with increases in the $ALDH^{high}$ cell population and number of spheroids. Inhibition of endogenous Akt by LY294002 resulted in decreased expression of Sox2, ALDH1, and CD133, leading to enhancement of $CoCl_2$-mediated apoptotic events due to altered ratio of bcl-2 to bax expression. These findings suggest that Ps lesions within GBM may serve as a specialized hypoxic niche, in which the HIF-1 α/pAkt axis is activated, in response to severe hypoxia.

Contents

1. Introduction

Glioma is the most common primary brain tumor, and includes low grade infiltrative astrocytomas (World Health Organization [WHO] grade II) and high grade tumors (grades III and IV). The highest grade (IV) of astrocytoma is also referred to as glioblastoma (GBM) [1]. The histopathological grading system for astrocytomas, which is based on nuclear pleomorphism and atypia, mitotic activity, vascular proliferation, and tumor necrosis, has clinical utility in predicting prognosis and determining the choice of treatment [2-4]. Low grade tumors are ultimately fatal but have substantially slower growth rates and impart longer survival (3-8 years), while the mean survival of GBM patients is a mere 14 weeks when patients receive only surgical resection, without adjuvant therapy[5-8].

It has been shown recently that astrocytoma is initiated and maintained by cancer stem cells (CSCs), a population of cells capable of extensive self-renewal, differentiation into multiple lineages, and recapitulation of the original tumor following grafting in immunodeficient mice[9,10]. CSCs are considered to be a cause of relapse and a promising cellular target in the development of novel therapeutic strategies [10-13]. Several distinct niches for CSCs, which provide a specialized microenvironment that maintains and regulates the properties of the resting cells, have been proposed in GBM, including perivascular and hypoxic regions [14-16].

Restricted oxygen conditions increase the CSC fraction and promote acquisition of a stem-like state [17,18]. All high grade astrocytomas contain numerous foci that are hypoxic and necrotic as compared to the surrounding brain tissue, since the rapidly growing astrocytomas outgrow the brain's vascular supply initially taken over by the tumor [19]. Necrotic foci are typically surrounded by pseudopalisading (Ps) cells, a configuration that is relatively unique to GBM and has long been recognized as an ominous prognostic feature [20,21]. Recent investigations have indicated that Ps lesions are severely hypoxic and overexpress hypoxia-inducible factor (HIF) [22,23], but little is known about the association between Ps features and CSC properties. In this study, we therefore examined the effects of hypoxia on the establishment and maintenance of CSC properties in Ps lesions within GBM, with emphasis on the status of HIF-1 α and its related molecules, as well as CSC-related markers, using *in vivo* and *in vitro* models.

2. Materials and methods

2-1. Clinical cases

A total of 110 cases of astrocytomas, surgically resected at the Kitasato University Hospital in the period from 1996 to 2013, were selected from our patient records, according to the criteria of the 2007 WHO classification [1]. The mean age of the patients was 49.2 years (range, 4 to 79 years). Of these, 25, 31, and 54 cases were subcategorized as grades II, III, and IV (primary, but not secondary, GBM), respectively. In the GBM cases, necrotic foci within tumor lesions were subdivided into two categories, necrosis with or without Ps features, which are characterized by an accumulation of tumor cells around a central necrosis zone (Supplementary Figure S1A). For evaluation of the necrotic area, the maximal internal width and height of each necrotic lesion were measured as described previously [20]. and the values of the necrotic areas were generated by multiplication of the two parameters. None of the patients were treated with chemo-radiation therapy before surgical resection of the tumors. All tissues were routinely fixed in 10% formalin and processed for embedding in paraffin wax. Approval for this study was given by the Ethics Committee of the Kitasato University School of Medicine (B13-28).

2-2. Antibodies and reagents

Anti-HIF-1 α, anti-$p27^{kip1}$, anti-bax, and anti-aldehyde dehydrogenase (ALDH)-1 antibodies were purchased from BD Biosciences (San Jose, CA, USA). Anti-bcl-2, anti-CD44s, and anti-Ki-67 antibodies were obtained from Dako (Copenhagen, Denmark). Anti-phospho-Akt at Ser473 (pAkt), anti-total Akt, anti-Oct4, anti-Slug, and anti-Snail antibodies were from Cell Signaling (Danvers, MA, USA). Anti-Glut-1, anti-CD133, and anti-survivin antibodies were purchased from Millipore (Billerica, MA, USA), Miltenyi Biotechnology (Bergisch Gladbach, Germany), and R&D Systems (Minneapolis, MN, USA), respectively. Anti-Sox2 and anti-β-actin antibodies were obtained from Abcam (Cambridge, MA, USA) and Sigma-Aldrich Chemicals (St Louis, MO, USA), respectively. LY294002 and cobalt chloride ($CoCl_2$) were purchased from Sigma Chemicals.

2-3. Immunohistochemistry

IHC was performed using a combination of the microwave-oven heating and polymer immunocomplex (Envision, Dako) methods, as described previously[24,25]. The immunoreactions were visualized with DAB (3,3' diaminobenzidine), and the nuclei were counterstained with methylgreen.

For evaluation of IHC findings, scoring of nuclear or cytoplasmic immunoreactivity for HNF-1α, Glut-1, pAkt, $p27^{Kip1}$, CD133, Sox2, CD44s, and ALDH1 was performed, as described previously [24,25]. Briefly, the proportion of immunopositive cells among the total number of counted cells was subdivided into five categories as follows: 0, all negative; 1, <10%; 2, 10-30%; 3, 30-50%; and 4, >50% positive cells. The immunointensity was also subclassified into four groups: 0, negative; 1, weak; 2, moderate; and 3, strong immunointensity. IHC scores were generated by multiplication of the values of the two parameters. Nuclear immunopositivity for Ki-67 was also counted in at least 500 cells in selected fields, including Ps and non-Ps lesions around the necrotic areas, as well as low and high HIF-1α areas. Labeling indices (LIs) were then calculated as number per 100 cells. Nuclear or cytoplasmic immunopositivity for Ki-67, bcl-2, and survivin was also counted in at least 500 cells in selected fields, including Ps and the surrounding tumor lesions. Based on the HIF-1α score, tumor lesions were also subdivided into two categories, as follows: low HIF-1α area, score < 2; high area, score$\geqq$2.

2-4. Apoptosis and TdT-mediated dUTP-biotin nick end-labeling assay

Apoptotic cells were identified in hematoxylin and eosin (HE)-stained sections, according to the criteria of Kerr et al [26]. Apoptotic indices (AIs) were calculated by counting the mean number of apoptotic figures per 10 high power fields. The *In Situ* Cell Death Detection Kit (Roche, Tokyo Japan) was also used for detection of apoptotic cells, according to the manufacturer's instructions. TUNEL-positive cells with the specific nuclear features were counted among at least 500 cells. Areas of severe inflammatory cell infiltration and necrosis were excluded, since questionable cells were observed in such lesions. LIs were then calculated as number per 100 cells.

2-5. Cell lines

Three astrocytoma cell lines, KS-1 (GBM), no. 10 (anaplastic astrocytoma), and KINGS-1 (anaplastic astrocytoma), which were obtained from the Health Science Research Resources Bank (Osaka, Japan), were maintained in Eagle's MEM or RPMI1640 with 10% bovine calf serum. For hypoxia experiments, cells were treated with 100 μM $CoCl_2$ under 5% CO_2 at 37 ℃, as described previously [25].

2-6. Western blot assays

Total cellular proteins were isolated using RIPA buffer [20 mM Tris-HCl (pH7.2), 1% Nonidet P-40, 0.5% sodium deoxycholate, 0.1% sodium dodecyl sulfate]. Aliquots of the proteins were resolved by SDS-PAGE, transferred to membranes, and probed with primary antibodies, coupled with the ECL detection system (Amersham Pharmacia Biotech., Tokyo, Japan).

2-7. Flow cytometry and Aldefluor assay

Individual cells were fixed using 70% alcohol and stained with propidium iodide (Sigma-Aldrich) for cell cycle analysis. Detached cells were also incubated with optimized antibodies, including anti-CD133 (Miltenyi Biotechnology), anti-mouse Immunoglobulin G-fluorescein isothiocyanate, or anti-mouse Immunoglobulin G-phycoerythrin obtained from BioLegend (San Diego, CA, USA). In addition, ALDH 1 enzyme activity in viable cells was determined using a fluorogenic dye based Aldefluor assay (Stem Cell Technologies, Grenoble, France), according to the manufacturer's instructions. The prepared cells were analyzed by flow cytometry using BD FACS Calibur (BD Biosciences) and CellQuest Pro software, version 3.3 (BD Biosciences).

2-8. Spheroid assay

Cells ($x10^3$) were plated in low cell binding plates (Thermo Fisher Scientific, Yokohama, Japan) in STK2 medium, a serum-free culture medium for mesenchymal stem cells [27], or Eagle's MEM with 10% bovine calf serum. Uniform spheroids with a minimum diameter of 50 μm were counted approximately two weeks following plating.

2-9. Statistics

Comparative data were analyzed using the Mann-Whitney *U*-test, the Spearman's correlation coefficient or the Kruskal-Wallis test, as appropriate. The cutoff for statistical significance was set as $p<0.05$.

3. Results

3-1. IHC findings in gliomas

In GBMs, the average values of necrotic areas were significantly lower in the lesions adjacent to Ps as compared to those lacking such features (Supplementary Figure S1B).

Representative images of IHC for HIF-1α, Glut-1, pAkt, $p27^{Kip1}$, and Ki-67, in GBM, as well as grade II and III astrocytomas, are illustrated in Figure 1A and Supplementary Figure S2, respectively. Distinct nuclear immunostaining for HIF-1α, $p27^{Kip1}$, and Ki-67 was observed, while Glut-1 expression was clearly cytoplasmic and pAkt was localized to both regions, demonstrating markedly heterogeneous distribution of the immunopositive astrocytoma cells within tumors.

Average IHC scores for Glut-1 and pAkt were significantly higher in the high HIF-1α lesions as compared to the low HIF-1α areas in grade II and III tumors and GBM. In the high HIF-1α group, HIF-1α, Glut-1, pAkt, and $p27^{Kip1}$ scores were significantly higher in GBM than in the grade II and III tumors, in contrast to a lack of such associations in the low HIF-1α category. In perinecrotic lesions within GBM, significantly higher IHC scores for HIF-1α, Glut-1, pAkt, and $p27^{Kip1}$ were observed in Ps lesions as compared to areas without Ps features. The Ki-67 LIs were significantly higher in the high HIF-1α category as compared to the low HIF-1α group in grade II and GBM cases. In addition, the LI values were also significantly lower in perinecrotic lesions with and without Ps features than in non-necrotic lesions in GBM (Figure 1B).

Representative images of IHC for several CSC markers, including CD133, Sox2, CD44s, and ALDH1, in GBM, as well as grade II and III astrocytomas, are illustrated in Figure 2A and Supplementary Figure S3, respectively. Cytoplasmic and/or membranous immunoreaction for CD133, CD44s, and ALDH1 and distinct nuclear immunostaining for Sox2 were observed in astrocytoma cells, particularly in the Ps lesions within GBM.

No differences in the IHC scores for CD133, Sox2, CD44s, and ALDH1 were observed between the low and high HIF-1α categories. In contrast,

significantly higher CD133, Sox2, CD44s, and ALDH1 scores were observed in perinecrotic Ps lesions as compared to perinecrotic lesions without Ps features and non-necrotic areas in GBM, as well as grade II and III tumors (Figure 2B).

As shown in Table 1, strongly positive correlations among the IHC scores for hypoxia-related molecules, including HIF-1α, pAkt, Glut-1, and $p27^{Kip1}$ were observed in all astrocytoma categories. Strongly positive correlations among IHC scores for CSC-related markers, such as CD133, Sox2, CD44s, and ALDH1, were also evident. In addition, positive correlations among hypoxia- and CSC-related molecules were also demonstrated, in contrast to a lack of any correlations of Ki-67 LIs with other markers. Similar findings were also found when examining grade II and III tumors and GBM categories separately (Supplementary Tables S1 and S2, respectively), with the exception of an association between HIF-1α score and Ki-67 LI in grade II and III tumors.

3-2. Relationship between hypoxia and stemness in glioma cells

The effects of $CoCl_2$ treatment on astrocytoma cell kinetics and stemness were examined, since it mimics the effects of hypoxia [25]. Treatment of KS-1 cells with low and moderate doses of $CoCl_2$ caused an increase in HIF-1α expression, in contrast to its inhibition by treatment with high doses (Supplementary Figure S4A). As shown in Figure 3A, short-term exposure of KS-1 cells to $CoCl_2$ abrogated growth considerably as compared to controls, leading to induction of G1-arrest during cell cycle progression. Expression of several hypoxia- and CSC-related molecules, including HIF-1α, $p27^{Kip1}$, pAkt, CD133, Sox2, and ALDH1, was also increased under hypoxic condition (Figure 3B). Aldefluor assay revealed an increase in the $ALDH^{high}$ cell population after $CoCl_2$ treatment, in line with the finding that showed a significantly increased number of well-defined, round spheroids that were over 50 μm in size (Figure 3C). Similar results were also observed in KINGS-1 and no. 10 cells (Supplementary Figure S4). Moreover, longterm exposure of KS-1 cells to $CoCl_2$ induced an alteration in cell morphology toward a fibroblast-like appearance which was observed after 90 days of treatment, along with increased expression of HIF-1α, Sox2, Oct4, Slug, and Snail (Figure 3D).

3-3. Inhibition of hypoxia-induced apoptosis by pAkt

Previous studies demonstrated that the CSC population can survive injury by preventing DNA damage through activation of the Akt signaling pathway [28]. To examine whether pAkt affects apoptosis and CSC status, KS-1 cells were treated with LY294002, an inhibitor of phosphatidylinositol 3' kinase (PI3K) which acts as an upstream effector of Akt. As shown in Figure 4A, treatment with $CoCl_2$ and/or LY294002 resulted in decreased bcl-2 and survivin expression, in contrast to no change in bax expression. LY294002 treatment also caused a decrease in expression of pAkt, Sox2, and ALDH1, but these inhibitory effects were abrogated by $CoCl_2$ treatment, with the exception of pAkt. In contrast, increased CD133 expression induced by $CoCl_2$ was apparently inhibited by LY294002 treatment (Figure 4A). TUNEL assay revealed that treatment of KS-1 cells with either $CoCl_2$ or LY294002 showed a significant increase in the amount of apoptotic cells. In addition, treatment with a combination of LY294002 and $CoCl_2$ resulted in further increase in apoptotic events (Figure 4B).

Apoptotic cells were readily detected in HE-stained sections on the basis of characteristic features, and the AIs were positively correlated with those detected by TUNEL assay (data not shown). Representative images of IHC for cytoplasmic bcl-2 and nuclear survivin in Ps lesions within GBM are illustrated in Figure 4C. The AI values were significantly higher in Ps lesions as compared to the surrounding areas, in contrast to significant decreases in both bcl-2 and survivin LIs in the former (Figure 4D). As shown in Table 2, AIs were inversely correlated with both bcl-2 and survivin LIs in Ps and the surrounding lesions, in contrast to a positive correlation between bcl-2 and survivin LIs.

4. Discussion

The present study clearly provided evidence that most astrocytomas contained numerous non-necrotic hypoxic foci that showed high expression of HIF-1 α and its related molecules. Interestingly, cell proliferation was significantly increased in high HIF-1 α lesions of grade II tumors and GBM as compared to the low HIF-1 α areas, while there was an overall lack of direct correlation between HIF-1 α score and Ki-67 LI. This may be due to the presence of Ps lesions with high HIF-1 α and low Ki-67, since a positive correlation (p= 0.4, $p<0.0001$) between the 2 was evident by exclusion of the data for these areas, indicating that Ps lesions may have specialized features in GBM tissues.

Given that embryonic day-12 rat mesencephalic precursor cells grown in a 3% oxygen environment exhibit increased proliferation and reduced apoptosis [29], it is suggested that a hypoxic microenvironment within tumors may contribute to tumor progression by activating an adaptive program that promotes tumor invasion and survival through activation of the HIF-1α signaling pathway. Further, significantly higher expression of HIF-1α and its related molecules was observed in high but not low HIF-1α lesions in GBM as compared to grade II and III tumors, which may be simply due to differences in oxygen levels among the tumors. In fact, it has been demonstrated that cellular hypoxia is mild (10% oxygen) and mild to moderate (10-2.5%) in grade II and III tumors, respectively, while it is severe (0.1%) in GBM [30].

Importantly, expression levels of HIF-1α and its related molecules were significantly higher in perinecrotic Ps lesions as compared to perinecrotic areas without Ps feature in GBM, which showed strongly positive correlations with pAkt status. In general, Ps lesions around necrotic regions appear to represent hypoxic tumor cells migrating away from vaso-occlusion and thrombosis [20,21]. In addition, Akt is believed to be involved in the epithelial-mesenchymal transition (EMT) pathway which leads to increased motility, reduced intercellular adhesion, and tumor progression [31]. Given that HIF-1α is regulated by the PI3K/Akt signal pathway [32], it appeared that activation of HIF-1α/Akt axis may contribute to the formation of Ps lesions within GBMs, and modulate astrocytoma cell movements under hypoxic condition. The lack of such findings in perinecrotic lesions without Ps features may be due to low viability of tumor cells, probably due to extremely severe hypoxia, since treatment of KS-1 cells with high doses of $CoCl_2$ resulted in decreased HIF-1α expression, in line with significantly lower HIF-1α score in non-Ps lesions. This conclusion may also be supported by the evidence that necrotic areas adjacent to Ps lesions were significantly smaller than those without Ps features.

Our results also showed that short-term treatment of astrocytoma cells with $CoCl_2$ was sufficient to induce CSC properties, along with an inhibition of cell proliferation, probably by promoting G1-arrest during cell cycle progression. This is in line with the evidence that oxygen availability regulates the tumor stem cell phenotype in GBM, and most hypoxic tumor cells are viable but non-proliferating[15,16,33]. By IHC, we demonstrated that the expression levels of several CSC-related markers were increased in Ps lesions with low cell proliferation activity within GBM, and were positively correlated to the expression of several hypoxia-related molecules. Given the results showing that

the expression of CSC-related markers was not increased in the non-necrotic regions as well as perinecrotic lesions without Ps features in GBM, it is suggested that Ps areas may contain key factors for generation or expansion of CSC properties.

Another interesting finding in this study was that long-term exposure of KS-1 cells with $CoCl_2$ resulted in not only an induction of EMT-like features, including alteration in morphology toward a fibroblast-like appearance and an increase in the expression of EMT-related molecules such as Slug and Snail, but also increased expression of the CSC-related markers, Sox2 and Oct4. Given that cells undergoing EMT exhibit stem cell-like traits and CSCs acquire mesenchymal-like characteristics [34], it is likely that prolonged hypoxia may be an important factor for a phenotypic shift toward a more stem-like status, along with activation of the EMT phenomenon.

In order to verify the importance of the Akt pathway in the regulation of CSC features in Ps lesions, since the cytoplasmic tail of phosphorylated CD133 binds to the PI3K regulatory subunit p85, resulting in activation of the PI3K/Akt pathway and subsequent promotion of CSC properties, endogenous Akt was inhibited with LY294002 [35]. Using KS-1 cells, we found that increased CD133 expression by $CoCl_2$ treatment was apparently abrogated by LY294002. Moreover, inhibition of endogenous pAkt also caused a decrease in expression of Sox2 and ALDH1. Given that positive correlations were found by IHC between pAkt status and expression of CD133, Sox2, and ALDH1 in astrocytoma tissues, it is likely that there is crosstalk between the Akt pathway and the strictly regulated CSC signaling required for CSC maintenance in astrocytomas.

A previous study proposed that TUNEL positivity was not a specific marker for apoptotic cells, since DNA fragmentation is common in a variety of cell deaths, including apoptosis, necrosis, and autolysis [36]. In this study, the AIs detected by specific nuclear features in HE-stained sections were positively correlated with TUNEL positivity, in line with our previous data [37]. In agreement with other studies [20,21], a significantly increased amount of apoptotic cells was observed in Ps lesions as compared to the surrounding areas in GBM, which was inversely correlated with bcl-2 and survivin expression. Treatment of KS-1 cells with $CoCl_2$ also caused an increase in the number of apoptotic cells and a decrease in bcl-2 but not bax expression, in line with the idea that a decrease in the ratio of bcl-2 to bax is essential for the induction of the mitochondrial-dependent apoptotic pathway[38]. Moreover, inhibition of endogenous pAkt by LY294002 resulted in further increase in $CoCl_2$-mediated

apoptosis. Therefore, it appeared that Akt may contribute to suppression of hypoxia-mediated apoptotic events induced by changes in bcl-2, survivin, and bax expression in Ps lesions within GBM.

Together, our observations provide evidence for a biological role of the HIF-1 α/pAkt axis in Ps lesions within GBM (Figure 5). (1) Increased cell proliferation triggers mild hypoxia due to relatively decreased blood supply, leading to upregulation of HIF-1 α and its related molecules. (2) Severe hypoxia, probably due to vascular occlusion, causes formation of Ps lesions around massive necrotic foci through activation of the HIF-1 α/pAkt axis. (3) Prolonged hypoxia plays a key role in promoting crosstalk among the HIF-1 α/pAkt axis and EMT- and CSC-related signaling networks required for CSC maintenance. (4) A hypoxic microenvironment may also promote the mitochondrial-dependent apoptotic pathway in some astrocytoma cells.

In conclusion, the present study provides evidence that Ps lesions within GBM may serve as a specialized microenvironment by acting as a hypoxic niche, in which the HIF-1 α/pAkt axis is activated, in response to severe hypoxia and promote CSC features in GBM.

5. Conclusion

Ps lesions within GBM may serve as a specialized microenvironment by acting as a hypoxic niche, in which the HIF-1 α/pAkt axis is activated, in response to severe hypoxia and promote CSC features in GBM.

6. Further study

To establish molecular target therapy for GBM cells in Ps lesions, several proteins, which were specifically overexpressed in the lesions, were detected by shot-gun proteomics methods using several samples of GBM with Ps lesions. In the present time, the biological roles of the molecules in GBMs are examined by *in vivo* and *in vitro* approach.

7. Acknowledgements

I am grateful to Professors T Kumabe and M Saegusa for the generous research guidance. I also thanks to members in Neurosurgery and Pathology

sections for the technical supports.

8. References

[1] Scheithauer BW, Hawkins C, Tihan T, VandenBerg SR, Burger PC. Astrocytic tumours. In: Louis DN, Ohgaki H, Wiestler OD, Cavenee WK, editors. WHO Classification of Tumours of the Central Nervous System, 4th ed. Lyon; 2007, p.13-52

[2] Daumas-Duport C, Scheithauer B, O'Fallon J, Kelly P. Grading of astrocytomas. A simple and reproducible method. Cancer 1988;62:2152-65.

[3] Kleihues P, Louis DN, Scheithauer BW, Rorke LB, Reifenberger G, Burger PC, et al. The who classification of tumors of the nervous system. J. Neuropathol. Exp Neurol 2002;61: 215-25.

[4] McCarthy BJ, Surawicz T, Bruner JM, Kruchko C, Davis F. Consensus conference on brain tumor definition for registration. Neurooncology 2002;4:134-45.

[5] Brat DJ, Castellano-Sanchez A, Kaur B, Van Meir EG. Genetic and biologic progression in astrocytomas and their relation to angiogenic dysregulation. Adv Anat Pathol 2002;9:24-36.

[6] Gupta M, Djalilvand A, Brat DJ. Clarifying the diffuse gliomas: an update on the morphologic features and markers that discriminate oligodendroglioma from astrocytoma. Am J Clin Pathol 2005;124:755-68.

[7] Bao S, Wu Q, McLendon RE, Hao Y, Shi Q, Hjelmeland AB, et al. Glioma stem cells promote radioresistance by preferential activation of the DNA damage response. Nature 2006;444:756-60.

[8] Sathornsumetee S, Rich JN. New treatment strategies for malignant gliomas. Expert Rev Anticancer Ther 2006;6:1087-104.

[9] Galli R, Binda E, Orfanelli U, Cipelletti B, Gritti A, De Vitis S, et al. Isolation and characterization of tumorigenic, stem-like neural precursors from human glioblastoma. Cancer Res 2004;64:7011-21.

[10] Singh SK, Hawkins C, Clarke ID, Squire JA, Bayani J, Hide T, et al. Identification of human brain tumour initiating cells. Nature 2004;432:396-401.

[11] Lapido T, Sirard C, Vormoor J, Murdoch B, Hoang T, Caceres-Cortes J, et al. A cell initiating human acute myeloid leukemia after transplantation into SCID mice. Nature 1994;367:645-8.

[12] Vescovi AL, Galli R, Reynolds BA. Brain tumour stem cells. Nat Rev 2006;6:425-36.
[13] Mao XG, Zhang X, Zhen HN. Progress on potential strategies to target brain tumor stem cells. Cell Mol Neurobiol 2009;29:141-55.
[14] Heddleston JM, Li Z, Lathia JD, Bao S, Hjelmeland AB, Rich JN. Hypoxia inducible factors in cancer stem cells. Br J Cancer 2010;102:789-95.
[15] Filatova A, Acker T, Garvalov. The cancer stem cell niche(s): the crosstalk between glioma stem cells and their microenvironment. Biochim Biophys Acta 2013;1830:2496-508.
[16] Calabrese C, Poppleton H, Kocak M, Hogg TL, Fuller C, Hamner B, et al. A perivascular niche for brain tumor stem cells. Cancer Cell 2007;11:69-82.
[17] Panchision DM. The role of oxygen in regulating neural stem cells in development and disease. J Cell Physiol 2009;220:562-8.
[18] Ezashi T, Das P, Roberts RM. Low O2 tensions and the prevention of differentiation of hES cells. Proc Natl Acad Sci USA 2005;102:4783-8.
[19] Peoch M, Farion R, Hiou A, Le Bas JF, Pasquier B, Remy C. Immunohistochemical study of vegf angiopoietin 2 and their receptors in the neovascularization following microinjection of C6 glioma cells into rat brain. Anticancer Res 2002;22:2147-51.
[20] Brat DJ, Castellano-Sanchez AA, Hunter SB, Pecot M, Cohen C, Hammond EH, et al. Pseudopalisades in glioblastoma are hypoxic, express extracellular matrix proteases, and are formed by an activity migrating cell population. Cancer Res 2004;64:920-7.
[21] Rong Y, Durden DL, Van Meir EG, Brat DJ. 'Pseudopalisading' necrosis in glioblastoma: a familiar morphologic feature that links vascular pathology, hypoxia, and angiogenesis. Neuropathol Exp Neurol 2006;65:529-39.
[22] Plate KH, Breier G, Weich HA, Risau W. Vascular endothelial growth factor is a potential tumour angiogenesis factor in human gliomas *in vivo*. Nature 1992;359:845-8.
[23] Shweiki D, Itin A, Soffer D, Kesher E. Vascular endothelial growth factor induced by hypoxia may mediate hypoxia-initiated angiogenesis Nature 1999;359:843-5.
[24] Saegusa M, Hashimura M, Kuwata T, Okayasu I. Requirement of the Akt/ β -catenin pathway for uterine carcinosarcoma genesis, modulating E-cadherin expression through the transactivation of *Slug*. Am J Pathol 2009;174:2107-15.

[25] Yoshida T, Hashimura M, Matsumoto T, Tazo Y, Inoue H, Kuwata T, et al. Transcriptional upregulation of HIF-1α by NF-κB/p65 and its associations with β-catenin/p300 complexes in endometrial carcinoma cells. Lab Invest 2013;93:1184-93.
[26] Kerr RJ, Winterford CM, Harmon BV. Apoptosis: its significance in cancer and cancer therapy. Cancer 1994;73:2013-26.
[27] Tsugeno Y, Sato F, Muragaki Y, Kato Y. Cell culture of human gingival fibroblasts, oral cancer cell and mesothelioma cells with serum-free media, STK1 and STK2. Biomed Rep 2014;2:644-8.
[28] Eyler CE, Foo WC, LaFiura KM, McLendon RE, Hjelmeland AB, Rich JN. Brain cancer stem cells display preferential sensitivity to Akt inhibition. Stem Cells 2008;26:3027-36.
[29] Studer L, Csete M, Lee SH, Kabbani N, Walikonis J, Wold B, et al. Enhanced proliferation, survival, and dopaminergic differentiation of CNS precursors in lowered oxygen. J Neurosci 2000;20:7377-83.
[30] Eavans SM, Judy KD, Dunphy I, Jenkins WT, Hwang WT, Nelson PT, et al. Hypoxia is important in the biology and aggression of human glial brain tumor. Clin Cancer Res 2004;10:8177-84.
[31] Bellacosa A, Kumar CC, Di Cristofano A, Testa JR. Activation of AKT kinases in cancer: implications for therapeutic targeting. Adv. Cancer Res 2005;94:29-86.
[32] Qiang L, Wu T, Zhang H-W, Lu N, Hu R, Wang Y-J, et al. HIF-1α is critical for hypoxia-mediated maintenance of glioblastoma stem cells by activating Notch signaling pathway. Cell Death Differ 2012;19:284-94.
[33] Bar EE, Lin A, Mahairaki V, Matsui W, Eberhart CG. Hypoxia increases the expression of stem-cell markers and promotes clonogenicity in glioblastoma neurospheres. Am J Pathol 2010;177:1491-502.
[34] Mani SA, Guo W, Liao MJ, Eaton EN, Ayyanan A, Zhou AY, et al. The epithelial-mesenchymal transition generates cells with properties of stem cells Cell 2008;133:704-15.
[35] Wei Y, Jiang Y, Zou F, Liu Y, Wang S, Xu N, et al. Activation of PI3K/Akt pathway by CD133-p85 interaction promotes tumorigenic capacity of glioma stem cells. Proc Natl Acad Sci USA 2013;110:6829-34.
[36] Grasl-Kraupp B, Ruttkay-Nedecky B, Koudelka H, Bukowska K, Bursch W, Schulte-Hermann R. *In situ* detection of fragmented DNA (TUNEL assay) fails to discriminate among apoptosis, necrosis, and autolytic cell death: a cautionary note. Hepatology 1995;21:1465-8.

[37] Tazo Y, Hara A, Onda T, Saegusa M. Bifunctional roles of survivin-ΔEx3 and survivin-2B for susceptibility to apoptosis in endometrial carcinomas. J Cancer Res Clin Oncol 2014;140:2027-7.
[38] Ling X, Cheng Q, Black JD, Li F. Forced expression of survivin-2B abrogates mitotic cells and induces mitochondria-dependent apoptosis by blockade of tubulin polymerization and modulation of bcl-2, bax, and survivin. J Biol Chem 2007;282:27204-14.

9. Accomplishments

Ⅰ) **Original articles :**

◯1. **Inukai M**, Hara A, Yasui Y, Kumabe T, Matsumoto T, Saegusa M : Hypoxia-mediated cancer stem cells in pseudopalisades with activation of hypoxia-inducible factor 1α/Akt axis in glioblastoma. Hum Pathol., 46(10):1496-1505, 2015.

2. Yoshida T, Hashimura M, Kuwata T, Matsumoto T, Suzuki E, **Inukai M**, et al : Transcriptional regulation of the alpha-1 type Ⅱ collagen gene by nuclear factor B/p65 and Sox9 in the chondrocytic phenotype of uterine cacinosarcomas. Hum Pathol., 44(9):1780-1788, 2013

3. Koizumi H, Utsuki S, **Inukai M**, Oka H, Osawa S, Fujii K : An operation in the park bench position complicated by massive tongue swelling. Case Rep Neurol Med., 2012:165860, 2012.

4. Kurata A, Suzuki S, Iwamoto K, Kakahara K, Abe K, **Inukai M**, et al : Altered hemodynamics associated with pathogenesis of the vertebral artery dissecting aneurysms. Stroke Res Treat., 2012:716919, 2012.

5. Miyajima Y, Oka H, Utsuki S, Hagiwara H, **Inukai M**, Kijima C, et al : Granulofilamentous meningioma. Brain Tumor Pathol., 30(1):57-60, 2013.

6. Kurata A, Suzuki S, Iwamoto K, **Inukai M**, Nakahara K, Satou K, et al : Efficacy of endovascular surgery for ruptured aneurysms with vasospasm of the parent artery. J Neurointerv Surg., 4(3):190-195, 2012.

7. Kurata A, Suzuki S, Iwamoto K, Nakahara K, **Inukai M**, Niki J, et al : A new transvenous approach to the carotid-cavenous sinus via the inferior petrooccipital vein. J Neurosurg., 116(3):581-587, 2012.

8. Kurata A, Suzuki S, Iwamoto K, Nakahara K, Sasaki M, **Inukai M**, et al : Dural arteriovenous fistulas in the cavernous sinus: clinical research and treatment. ISRN Neurol., 2011:453834, 2011.

9． Kurata A, Suzuki S, Iwamoto K., Miyazaki T, **Inukai M**, Abe K, et al：Direct-puncture approach to the extraconal portion of the superior ophthalmic vein for carotid cavernous fistulae. Neuroradiology, 51(11):755-759, 2009.

10． Yoshida S, Amano H, Hayashi I, Kitasato H, Kamata M, **Inukai M**, et al：COX-2/VEGF-dependent facilitation of tumor-associated angiogenesis and tumor growth in vivo. Lab Invest., 83(10):1385-1394, 2003.

11 Hayashi I, Amano H, Yoshida S, Kamata K, Kamata M, **Inukai M**, et al：Suppressed angiogenesis in kininogen-deficiencies. Lab Invest., 82(7):871-880, 2002.

Ⅱ）**Associate articles・Proceedings：**

none

Ⅲ）**Case reports：**

犬飼円，岡秀宏，佐藤澄人，宇津木聡，藤井清孝：ラトケのう胞術後に浸透圧性脱髄症候群となった一例．日本内分泌学会雑誌，86：54－56，2010.

Ⅳ）**Literary works：**

none

Ⅴ）**Review articles：**

none

Ⅵ）**Research reports：**

none

Ⅶ）**Conference presentations：**

〈General speech〉

1． 犬飼円，原敦子，安井美江，三枝信，隈部俊宏：Akt 系は膠芽腫の低酸素ニッチ環境のがん幹細胞化維持機構である．第 33 回日本脳腫瘍学会学術集会，京都(日本脳腫瘍学会学術集会 プログラム・抄録号：215-215, 2015．）

2． 犬飼円，原敦子，橋村美紀，鶴田智子，安井美江，三枝信：Akt 系は膠芽腫の低酸素ニッチ環境のがん幹細胞化維持機構である. 第 104 回日本病理学会総会，2015，名古屋.（日本病理学会総会抄録号：91-91，2015．）

３．　犬飼円，眞野唯，長南雅志，関口朋子，大澤成之，宮島良輝，他：BCNU wafer 貼付後の組織変化:再手術例と剖検例より. 第 32 回日本脳腫瘍病理学会, 2014, 徳島．(The 32nd Annual Meeting of the Japanese Society of Brain Tumor Pathology，: 33-33，2014．)

４．　犬飼円，原敦子，橋村美紀，鶴田智子，三枝信：膠芽腫の偽柵状配列部内低酸素ニッチ環境で生じるがん幹細胞様変化の証明．第 103 回日本病理学会総会，2014，広島．(日本病理学会総会抄録号：49-49，2014．)

５．　犬飼円，原敦子，柳澤信之，三枝信：脳生検の一例．第 98 回神奈川県病理医会，2014，相模原．(神奈川医学会雑誌，41(2)：184-185，2014．)

６．　犬飼円，原敦子，橋村美紀，鶴田智子，三枝信：グリオーマの低酸素環境依存性組織再構築．第 102 回日本病理学会総会，2013，札幌．(日本病理学会総会抄録号：73-73，2013．)

７．　犬飼円，中原邦晶，岡秀宏，金子忠弘，今野慎吾，北原孝雄，他：頭部外傷後、脳静脈洞血栓を生じた二症例．第 40 回日本小児神経外科学会，2012，岡山．(小児の脳神経，37(2)：207-207，2012．)

８．　犬飼円，倉田彰，鈴木祥生，佐々木亮，湯沢泉，岩本和久，他：エンタープライズステントのみで治療し得た内頚動脈前壁動脈瘤の一例．第 27 回日本脳神経血管内治療学会学術総会，2011，千葉．(脳神経血管内治療，5(4)：337-337，2011．)

９．　犬飼円，倉田彰，岩本和久，仁木淳，中原邦晶，佐藤公俊，他：海綿静脈洞への新しい経静脈的アプローチルート．第 26 回日本脳神経血管内治療学会学術総会，2010，小倉．(脳神経血管内治療，4(4)：270-270，2010．)

１０．犬飼円，中原邦晶，岡秀宏，宇津木聡，藤井清孝：骨性 human tail を伴った pfeiffer 症候群の一例．第 38 回日本小児神経外科学会，2010，富山．(小児の脳神経，35(2)：280-280，2010．)

１１．犬飼円，岡秀宏，佐藤澄人，宇津木聡，藤井清孝：ラトケのう胞術後に浸透圧性脱髄症候群となった一例．第 22 回内分泌外科学会，2010，名古屋．(日本内分泌学会雑誌，86：54-56，2010．)

１２．犬飼円，岡秀宏，佐藤澄人，宇津木聡，藤井清孝：ラトケのう胞術後に浸透圧性脱髄症候群となった一例．第 20 回日本間脳下垂体学会，2010，神戸．(日本内分泌学会雑誌，86：54-56，2010．)

１３．犬飼円，倉田彰，鈴木祥生，岩本和久，中原邦晶，仁木淳，他：腕頭動脈起始

部狭窄症に対してステント留置術を施行した 1 例. 第 110 回日本脳神経外科学会関東支部総会，2009，東京.（PDF，: B27，2009.）

１４．犬飼円，倉田彰，鈴木祥生，宮崎朋子，馬渕一樹，阿部克智，他：異なる部位に新たに出現した De-novo dAVF の二例. 第 25 回日本脳神経血管内治療学会学術総会，2009，富山.（脳神経血管内治療，3(4)：374-374，2009.）

１５．犬飼円，倉田彰，鈴木祥生，岩本和久，大澤成之，宮崎朋子，他：大型石灰化動脈瘤に対する塞栓術. 第 24 回日本脳神経血管内治療学会学術総会，2008，名古屋.（脳神経血管内治療，2(4)：207-207，2008.）

Ⅷ）**Public lectures・Educational lectures：**

none

Ⅸ）**Reserch funding acquisition：**

1. 犬飼円：平成 26 年度院生プロジェクト研究(北里大学医療系研究科大学院)，膠芽腫の低酸素ニッチ領域におけるがん幹細胞化制御機構の解明，40 万円，2014～2015
2. 犬飼円：平成 26 年度若手医師および医療従事者研究助成金(株式会社エスアールエル)，膠芽腫の低酸素環境による癌幹細胞化誘導の分子機構の解明，40 万円，2014～2015
3. 犬飼円：2013 年度若手研究者研究助成金(キャタピラージャパン株式会社)，膠芽腫の低酸素関連シグナル系による増殖制御・組織再構築機構の解明と新規治療法への展開，40 万円，2013～2014
4. 犬飼円：平成 25 年度院生プロジェクト研究(北里大学医療系研究科大学院)，膠芽腫の低酸素関連シグナルネットワークによる増殖制御の分子機構の解明と新規治療法への応用，40 万円，2013～2014
5. 犬飼円：平成 24 年度医学部けやき会研究助成金(北里大学医学部けやき会)，悪性グリオーマの低酸素関連シグナル系による増殖制御・組織再構築機構の解明と新規治療法への展開，25 万円，2012～2013

10. Figures and tables

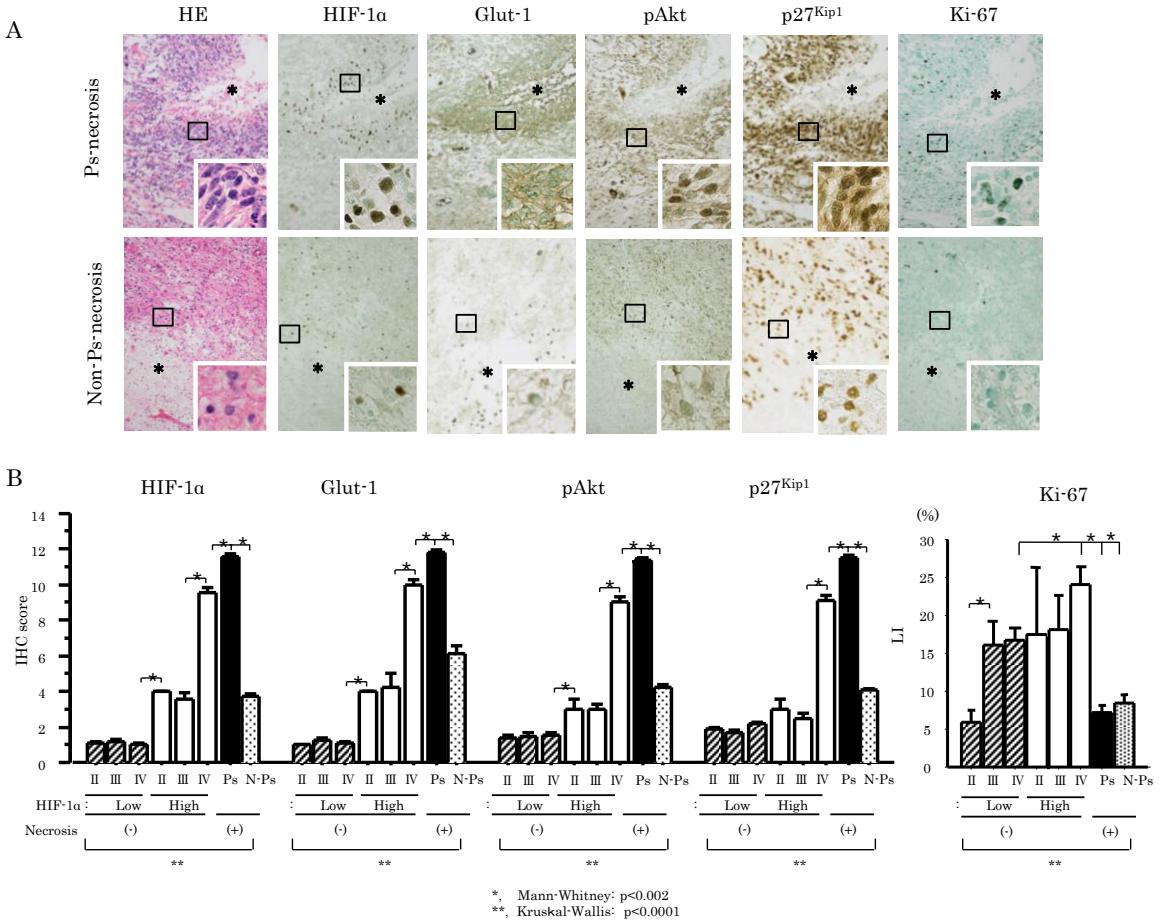

Figure 1. IHC findings in serial sections of GBMs. A, Staining is for HE and by IHC for the indicated molecules in Ps (upper panel) and perinecrotic lesion without Ps feature (lower panel). Closed boxes are magnified in the insets. Asterisk, necrotic areas within tumors. Original magnification, x200 and x400 (inset). B, IHC scores and Ki-67 LIs for the indicated molecules in low and high HIF-1α lesions in grades II and III tumors and GBM, as well as perinecrotic lesions with or without pseudopalisades (Ps or N-Ps). The data shown are means±SD.

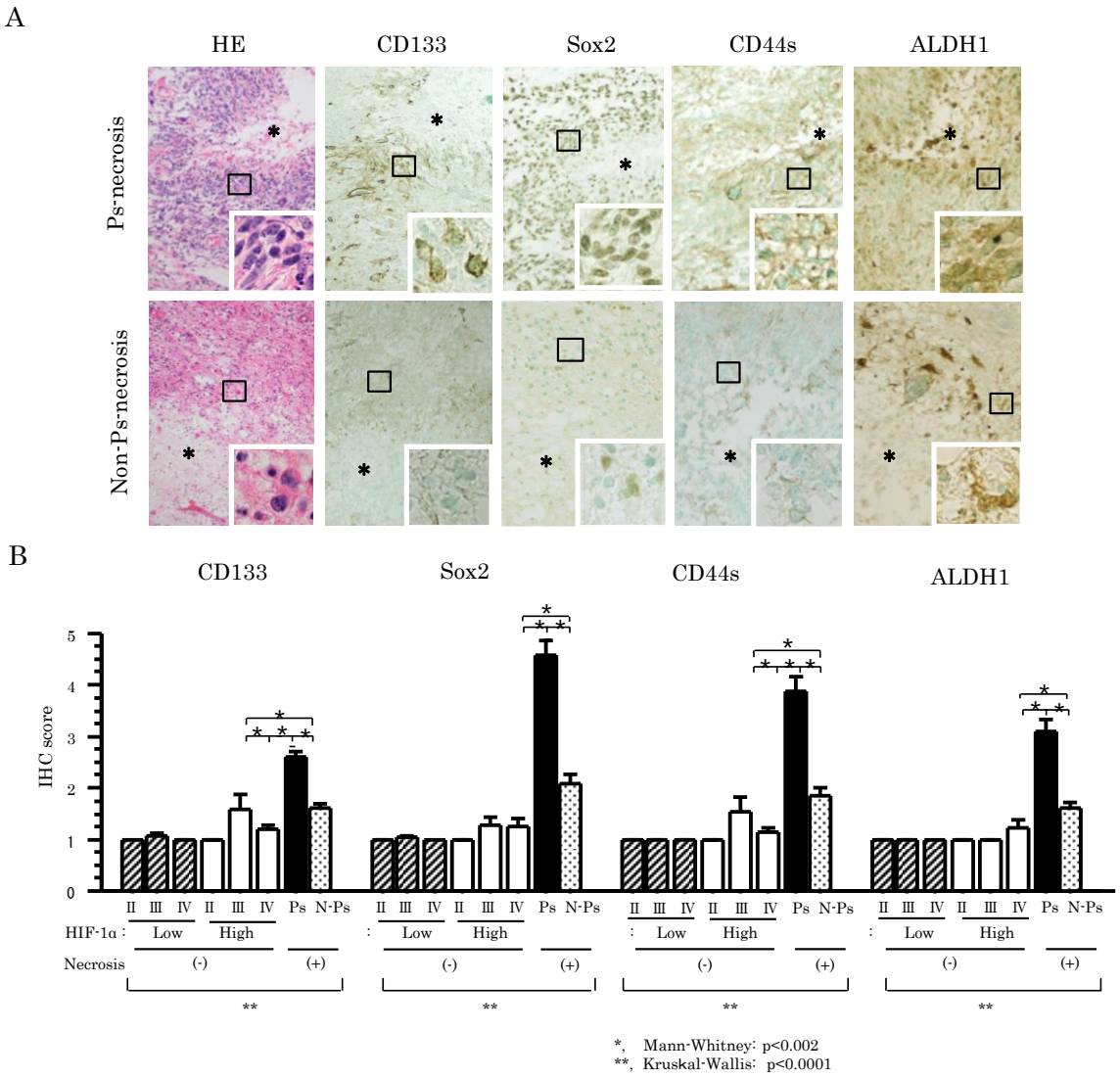

Figure 2. IHC findings in serial sections of GBM. A, Staining is for HE and by IHC for the indicated molecules in Ps (upper panel) and perinecrotic lesions without Ps features (lower panel). Closed boxes are magnified in the insets. Asterisk, necrotic areas within tumors. Original magnification, x200 and x400 (inset). B, IHC scores for the indicated molecules in low and high HIF-1α lesions in grades II and III tumors and GBM, as well as perinecrotic lesions with or without pseudopalisades (Ps or N-Ps). The data shown are means±SD.

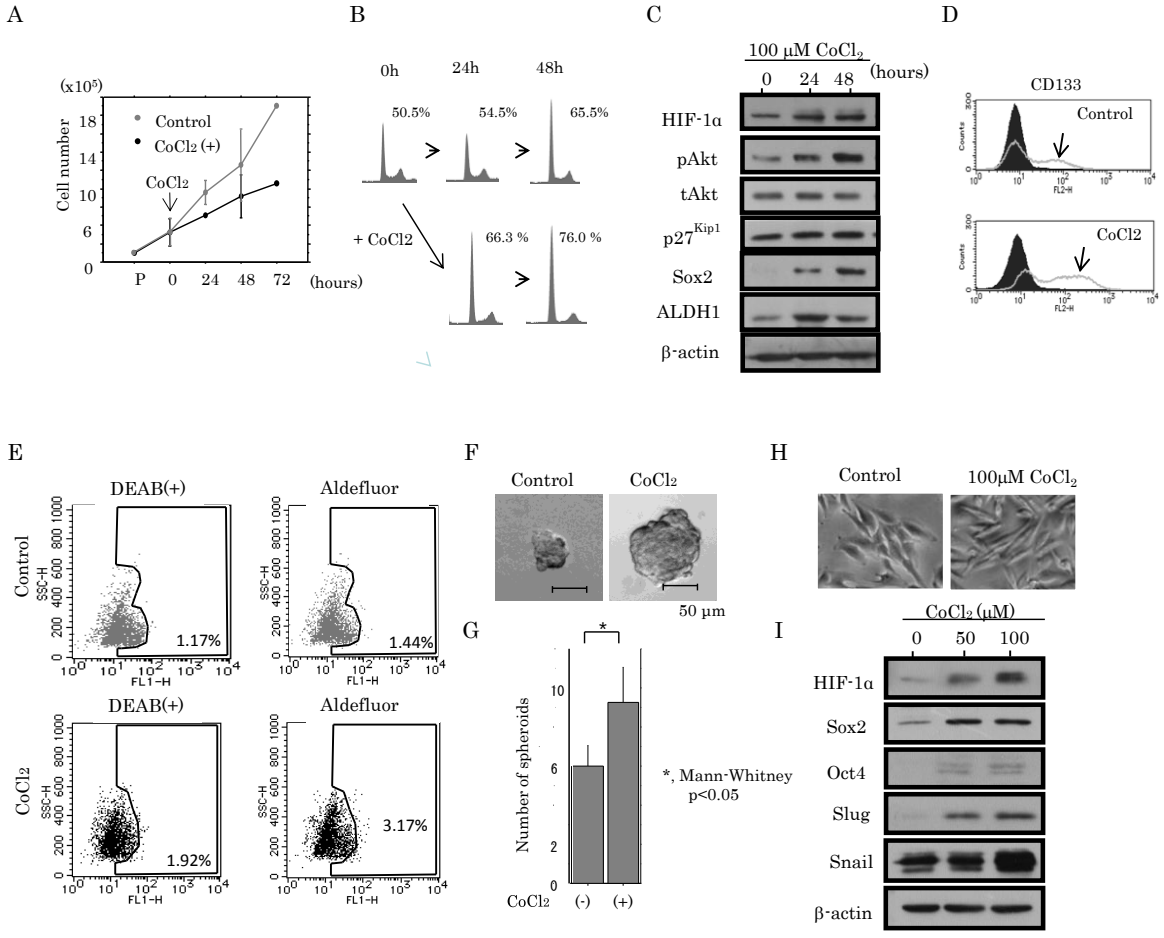

Figure 3. Relationship between hypoxia and CSC properties in GBM cells. A, KS-1 cells were seeded at low density with or without 100 μM $CoCl_2$ treatment for the time shown. The cell numbers are presented as means±SD. P, cell passage. B, Cell cycle analysis by flow cytometry of KS-1 cells with or without 100 μM $CoCl_2$ treatment for the time shown. C, Western blot analysis of the indicated molecules after exposure to 100 μM $CoCl_2$ in KS-1 cells for the time shown. D, KS-1 cells were stained for CD133 after 100 μM $CoCl_2$ treatment for 24 hours. Note the increased CD133-positive population in the group treated with 100 μM $CoCl_2$ (indicated by arrows). E, Aldefluor analysis in KS-1 cells with or without 100 μM $CoCl_2$ treatment. "DEAB" denotes diethylaminobenzaldehyde. F, Phase-contrast images of KS-1 cell spheroids after treatment with 100 μM $CoCl_2$ for 14 days. G, The number of spheroids is presented as means±SD. H, Phase-contrast images of KS-1 cells treated with 100 μM $CoCl_2$ for 90 days. Note the fibroblast-like appearance of the KS-1 cells. I, Western blot analysis of the indicated molecules after prolonged exposure to 50 and 100 μM $CoCl_2$ in KS-1 cells for 90 days.

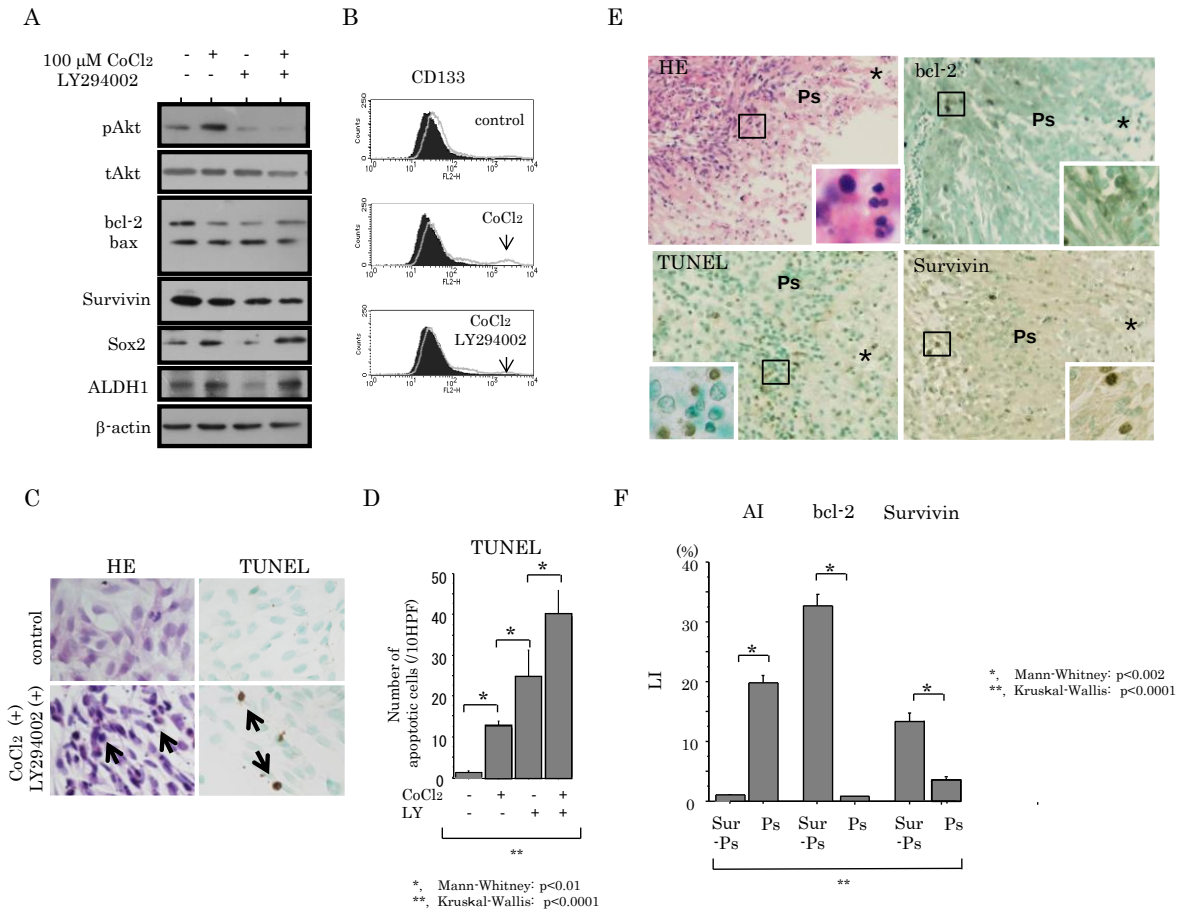

Figure 4. Association between pAkt expression and apoptosis in GBM. A, Western blot analysis of the indicated molecules after treatment with 100 μM $CoCl_2$ and 20 μM LY294002 in KS-1 cells for 24 hours. B, KS-1 cells were stained for CD133 after treatment with 100 μM $CoCl_2$ and/or 20 μM LY294002 for 24 hours. Note the increased CD133-positive population in the group treated with 100 μM $CoCl_2$, in contrast to a decrease in this population in the group treated with 20 μM LY294002 (indicated by arrows). C, After treatment with 100 μM $CoCl_2$ and/or 20 μM LY294002 for 24 hours, KS-1 cells undergoing apoptosis (indicated by arrows) were detected in HE sections (left) and by the TUNEL assay (right). Original magnification, x400. D, Apoptotic cells detected by the TUNEL assay among KS-1 cells treated with 100 μM $CoCl_2$ and/or 20 μM LY294002 for 24 hours. E, Detection of apoptotic cells in HE section (upper left) and by the TUNEL assay (lower left) and staining by IHC for bcl-2 (upper right) and survivin (lower right) in Ps around necrotic regions (indicated by asterisk) in GBM. Closed boxes are magnified in the insets. Original magnification, x200 and x400 (inset). F, AI and LIs for bcl-2 and survivin in Ps and the surrounding tumor lesions (Sur-Ps). The data shown are means±SD.

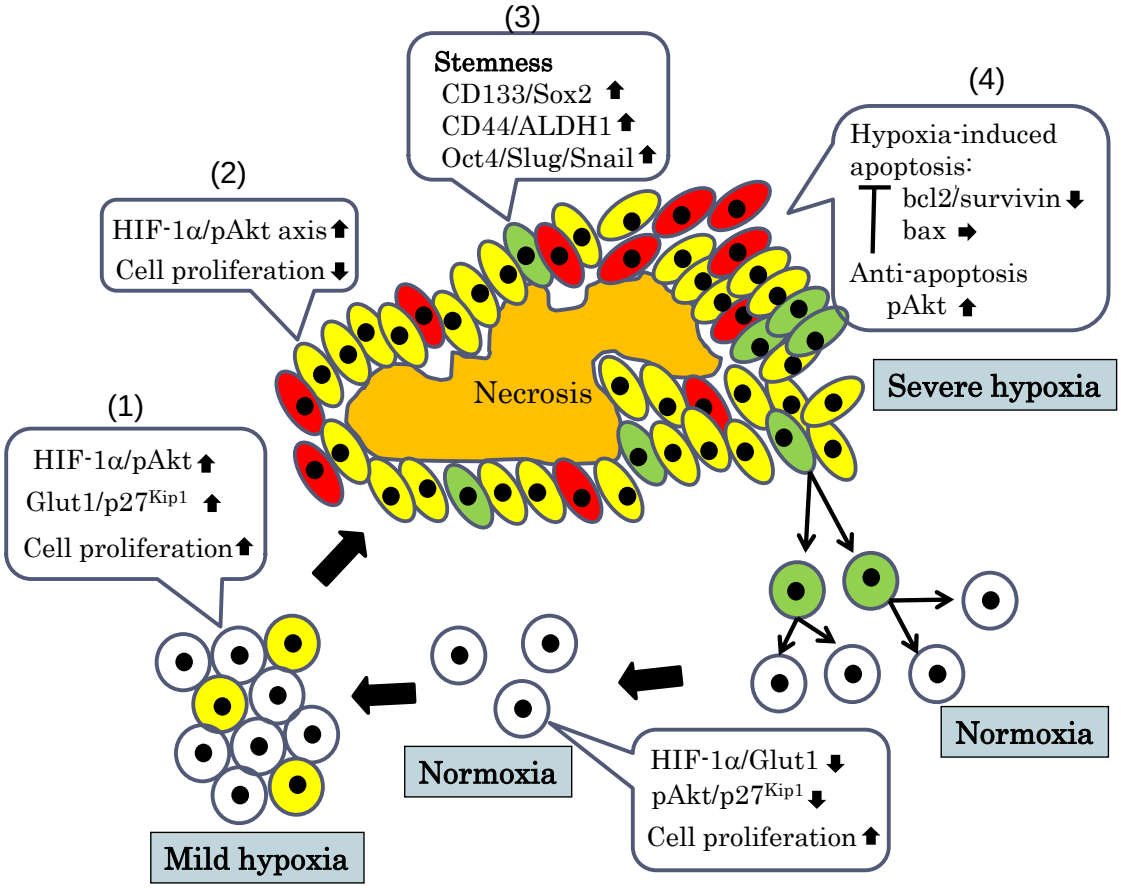

Figure 5. Schematic representation of associations among pseudopalisading necrosis, HIF-1 α /pAkt axis, and CSC properties in GBM.

Table 1.

Correlations among hypoxia- and CSC-related markers investigated in astrocytomas

	HIF-1α ρ (p)	Glut-1 ρ (p)	pAkt ρ (p)	$p27^{Kip1}$ ρ (p)	Ki-67 ρ (p)	CD133 ρ (p)	Sox2 ρ (p)	CD44s ρ (p)
Glut-1	0.91 (<0.0001)	*	*	*	*	*	*	*
pAkt	0.91 (<0.0001)	0.89 (<0.0001)	*	*	*	*	*	*
$p27^{Kip1}$	0.9 (<0.0001)	0.86 (<0.0001)	0.91 (<0.0001)	*	*	*	*	*
Ki-67	0.08 (0.18)	−0.72 (0.7)	0.02 (0.79)	0.06 (0.29)	*	*	*	*
CD133	0.61 (<0.0001)	0.63 (<0.0001)	0.59 (<0.0001)	0.61 (<0.0001)	0.03 (0.58)	*	*	*
Sox2	0.6 (<0.0001)	0.66 (<0.0001)	0.6 (<0.0001)	0.6 (<0.0001)	−0.16 (0.78)	0.85 (<0.0001)	*	*
CD44s	0.62 (<0.0001)	0.66 (<0.0001)	0.62 (<0.0001)	0.63 (<0.0001)	0.03 (0.67)	0.87 (<0.0001)	0.92 (<0.0001)	*
ALDH1	0.61 (<0.0001)	0.66 (<0.0001)	0.62 (<0.0001)	0.63 (<0.0001)	0.07 (0.25)	0.8 (<0.0001)	0.92 (<0.0001)	0.87 (<0.0001)

Abbreviations: CSC, cancer stem cells; ρ, Spearman's correlation coefficient

Table 2.

Relationship between AI and expression levels of bcl-2 and survivin in Ps lesions in GBM

	AI ρ (p)	bcl-2 ρ (p)
bcl-2	-0.7 (<0.0001)	*
Survivin	-0.38 (<0.0001)	0.48 (<0.0001)

Abbreviations: AI, apoptotic index; Ps, pseudopalisade; GBM, glioblastoma;ρ , Spearman correlation coefficient.

A

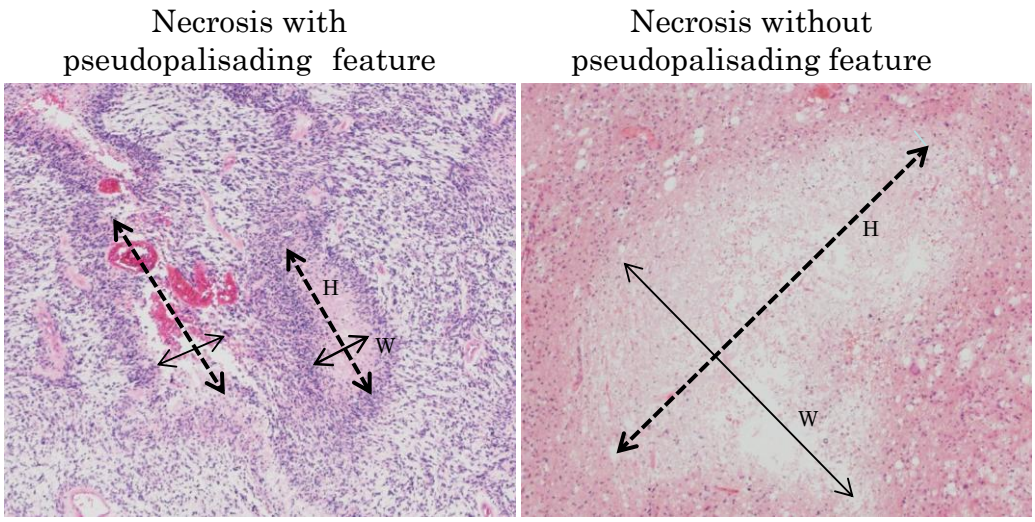

B

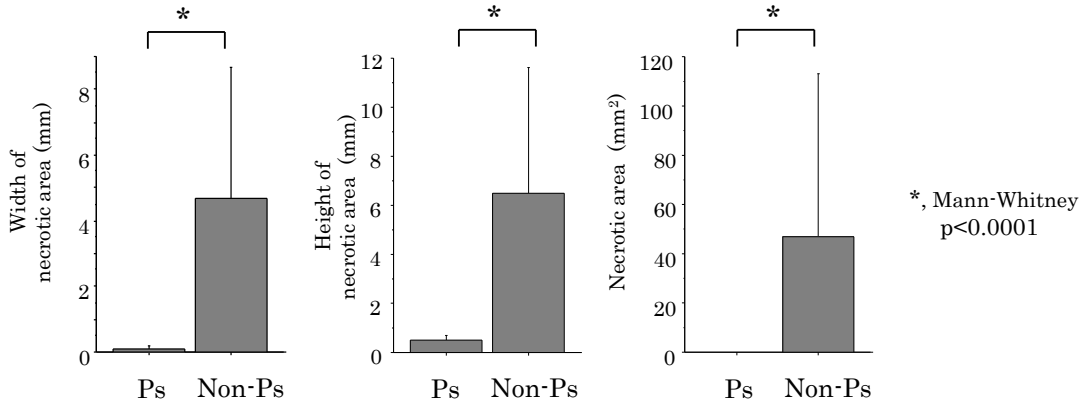

Supplementary Figure S1. Representation of necrotic areas in GBM. A, Necrosis (indicated by asterisk) with and without Ps features (indicated by arrows) in GBM. Measurements for greatest internal height (H) and greatest internal width (W) of necrotic areas with or without Ps features. Original magnification x200. B, The values for the greatest internal width (left) and the greatest internal height (middle) in necrotic lesions. The necrotic areas with or without pseudopalisades are generated by multiplication of the wigth and the height (right). The data shown are means±SD.

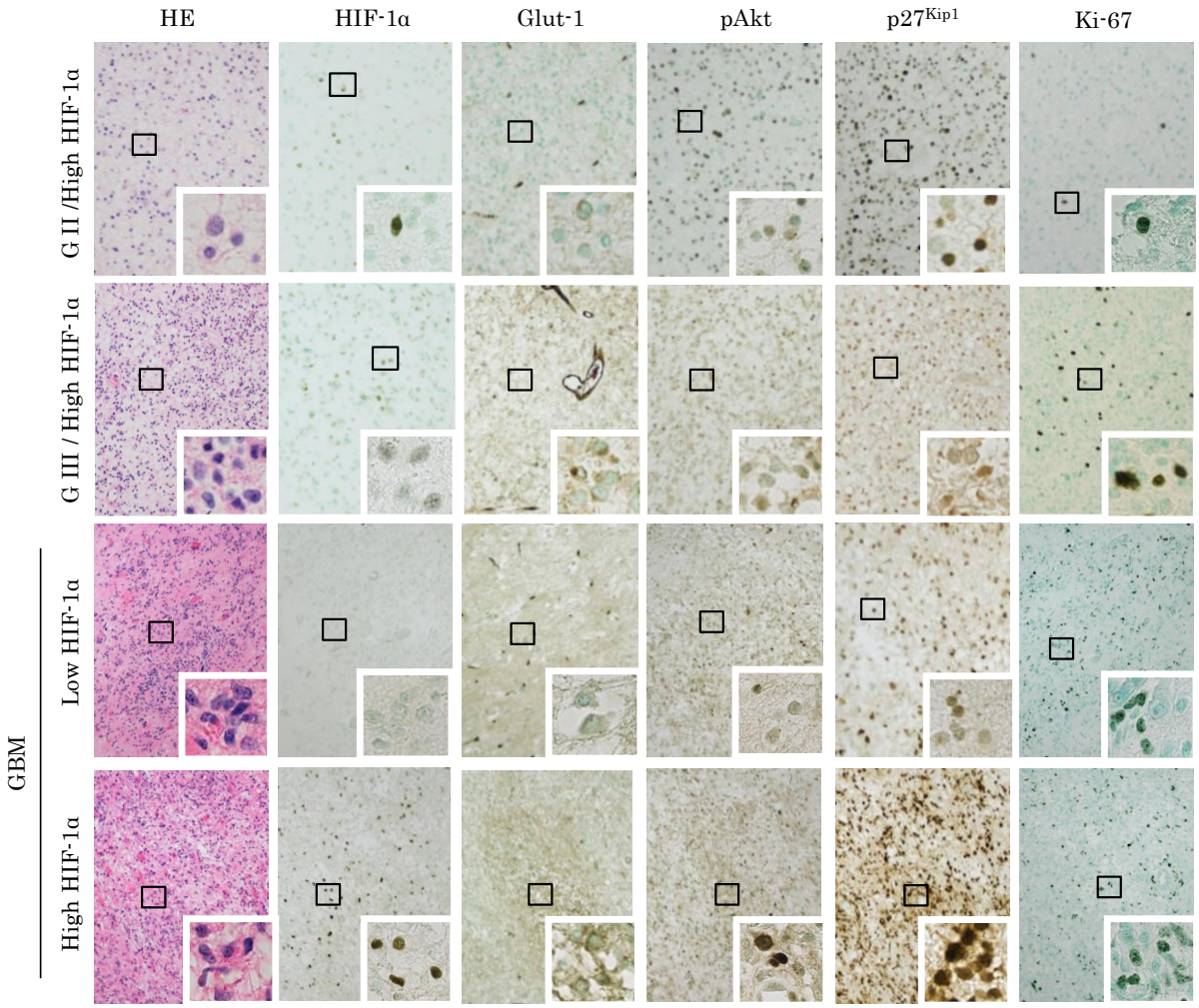

Supplementary Figure S2. IHC findings in serial sections of grades II and III tumors and GBM. Staining is for HE and by IHC for the indicated molecules in high HIF-1 α areas in grades II and III tumors and GBM. Closed boxes are magnified in the insets. Original magnification, x200 and x400 (inset).

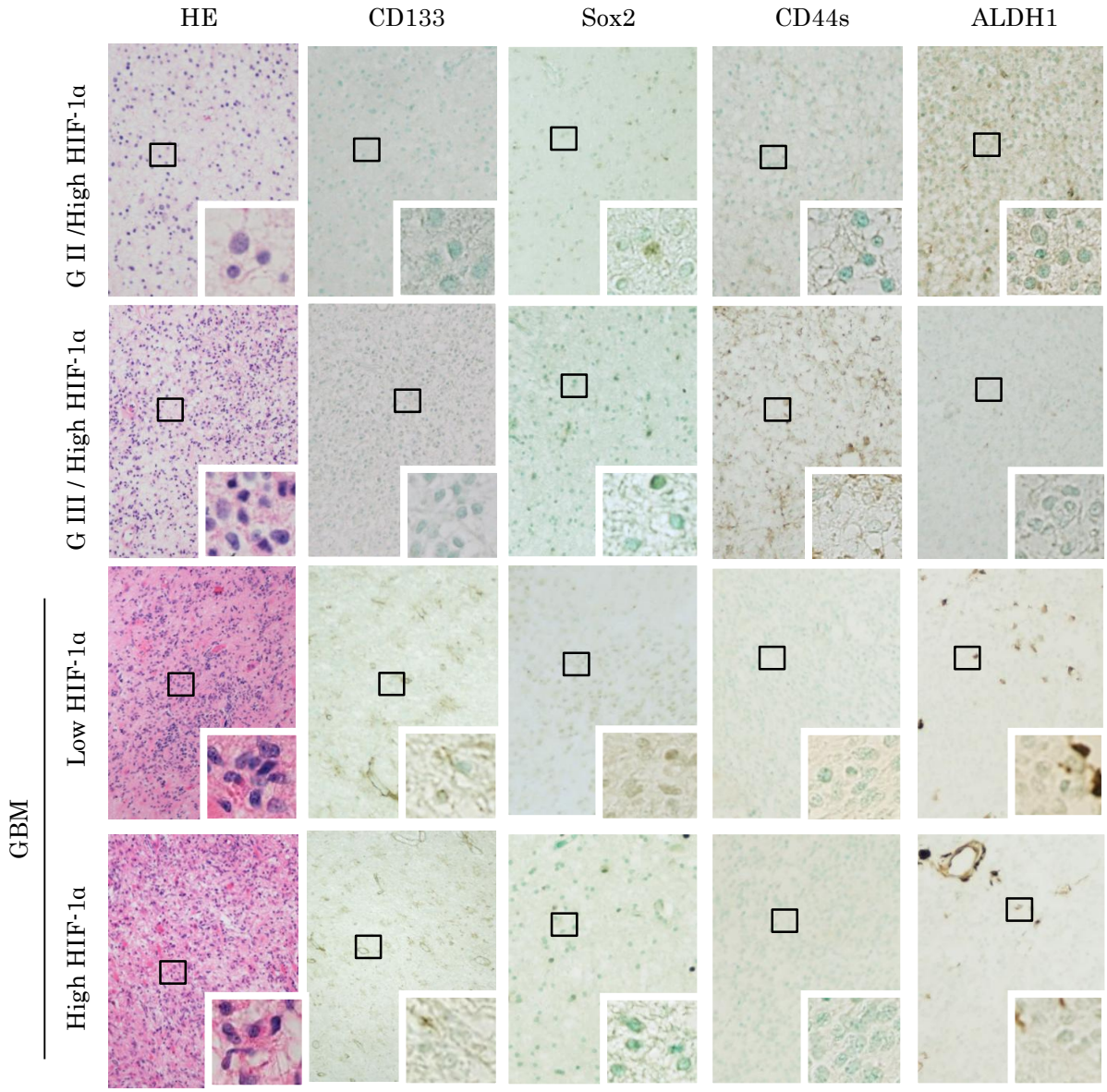

Supplementary Figure S3. IHC findings in serial sections of grade II and III tumors and GBM. Staining is for HE and by IHC for the indicated molecules in high HIF-1 α areas in grade II and III tumors and GBM. Closed boxes are magnified in the insets. Original magnification, x200 and x400 (inset).

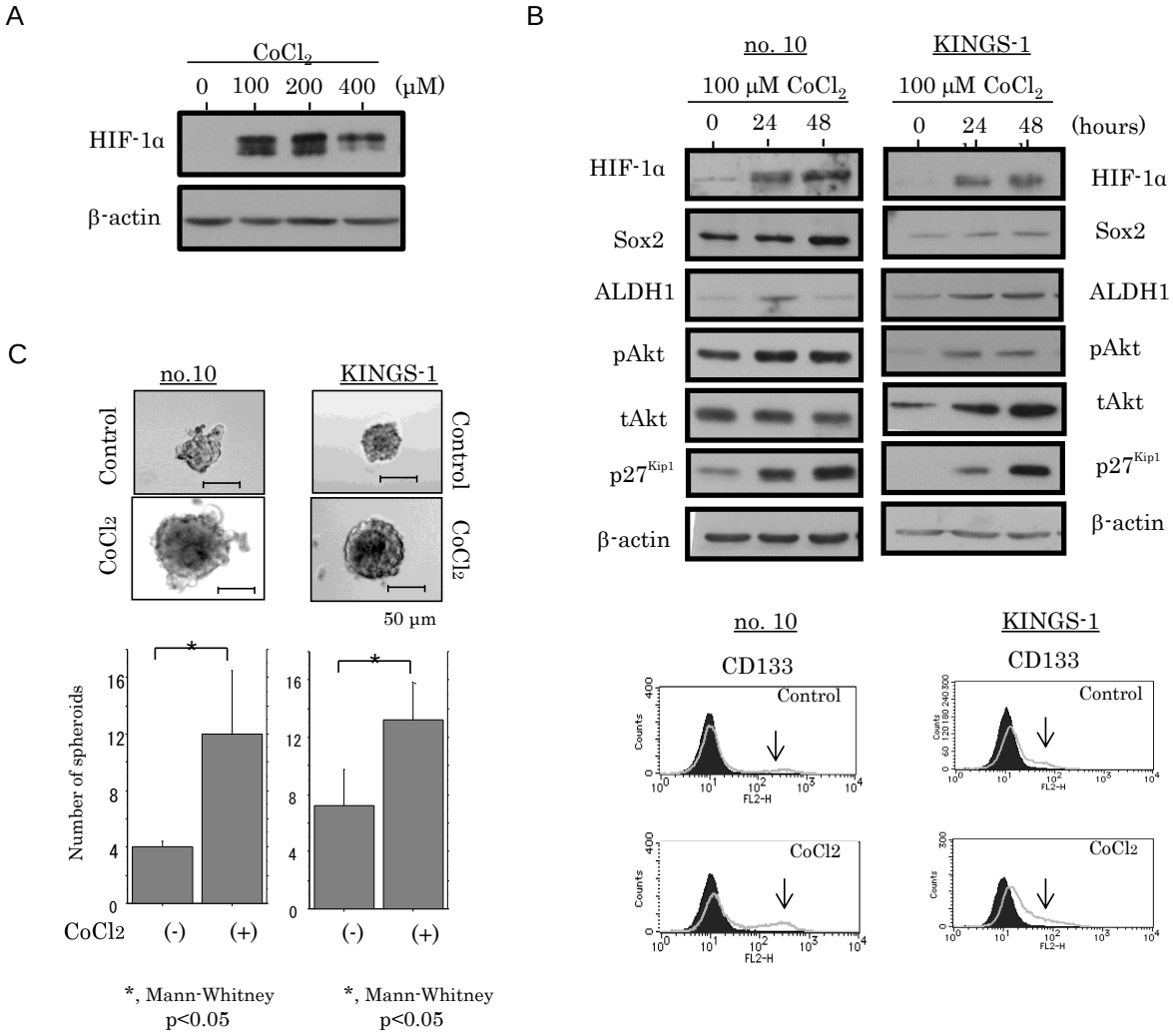

Supplementary Figure S4. Relationship between hypoxia and CSC properties in glioma cells. A, Western blot analysis of HIF-1α after treatment with 100, 200, and 400 μM $CoCl_2$ in KS-1 cells 24 hours. B, Upper: Western blot analysis of the indicated molecules after exposure to 100 μM $CoCl_2$ in no. 10 and KINGS-1 cells for the time shown. Lower: KS-1 cells were stained for CD133 after 100 μM $CoCl_2$ treatment for 24 hours. Note the increased CD133-positive population in the group treated with 100 μM $CoCl_2$ (indicated by arrows) for 24 hours. C, Upper: phase-contrast images of no. 10 and KINGS-1 cells treated with 100 μM $CoCl_2$ treatment for 2 weeks. Lower: the number of spheroids is presented as means±SD.

Supplementary Table S1.

Correlations among hypoxia- and cancer stem cell-related markers investigated in grade II and III astroctyomas

	HIF-1α ρ (p)	Glut-1 ρ (p)	pAkt ρ (p)	$p27^{Kip1}$ ρ (p)	Ki-67 ρ (p)	CD133 ρ (p)	Sox2 ρ (p)	CD44s ρ (p)
Glut-1	0.75 (<0.0001)	*	*	*	*	*	*	*
pAkt	0.67 (<0.0001)	0.65 (<0.0001)	*	*	*	*	*	*
$p27^{Kip1}$	0.49 (<0.0001)	0.45 (<0.0001)	0.48 (<0.0001)	*	*	*	*	*
Ki-67	0.39 (0.0005)	0.27 (0.01)	0.23 0.13	0.16 (0.14)	*	*	*	*
CD133	0.65 (<0.0001)	0.69 (<0.0001)	0.55 (<0.0001)	0.61 (<0.0001)	0.38 (0.0008)	*	*	*
Sox2	0.63 (<0.0001)	0.74 (<0.0001)	0.5 (<0.0001)	0.57 (<0.0001)	0.38 (0.0008)	0.93 (<0.0001)	*	*
CD44s	0.64 (<0.0001)	0.71 (<0.0001)	0.53 (<0.0001)	0.59 (<0.0001)	0.45 (<0.0001)	0.94 (<0.0001)	0.97 (<0.0001)	*
ALDH1	0.63 (<0.0001)	0.73 (<0.0001)	0.58 (<0.0001)	0.061 (<0.0001)	0.5 (0<0.0001)	0.88 (<0.0001)	0.91 (<0.0001)	0.95 (<0.0001)

ρ, Spearman's correlation coefficient

Supplementary Table S2.

Correlations among hypoxia- and cancer stem cell-related markers investigated in GBMs

	HIF-1α ρ (p)	Glut-1 ρ (p)	pAkt ρ (p)	$p27^{Kip1}$ ρ (p)	Ki-67 ρ (p)	CD133 ρ (p)	Sox2 ρ (p)	CD44s ρ (p)
Glut-1	0.88 (<0.0001)	*	*	*	*	*	*	*
pAkt	0.92 (<0.0001)	0.88 (<0.0001)	*	*	*	*	*	*
$p27^{Kip1}$	0.93 (<0.0001)	0.93 (<0.0001)	0.93 (<0.0001)	*	*	*	*	*
Ki-67	−0.03 (0.69)	−0.15 (0.03)	−0.09 (0.21)	−0.17 (0.8)	*	*	*	*
CD133	0.56 (<0.0001)	0.59 (<0.0001)	0.54 (<0.0001)	0.57 (<0.0001)	−0.12 (0.1)	*	*	*
Sox2	0.53 (<0.0001)	0.6 (<0.0001)	0.55 (<0.0001)	0.53 (<0.0001)	−0.19 (0.007)	0.82 (<0.0001)	*	*
CD44s	0.55 (<0.0001)	0.62 (<0.0001)	0.56 (<0.0001)	0.57 (<0.0001)	−0.16 (0.02)	0.84 (<0.0001)	0.89 (<0.0001)	*
ALDH1	0.53 (<0.0001)	0.59 (<0.0001)	0.54 (<0.0001)	0.54 (<0.0001)	−0.11 (0.12)	0.78 (<0.0001)	0.91 (<0.0001)	0.84 (<0.0001)

ρ, Spearman's correlation coefficient